Computers and Geotechnics 69 (2015) 578–587

Contents lists available at ScienceDirect

Computers and Geotechnics

journal homepage: www.elsevier.com/locate/compgeo

Research Paper

Modelling of laboratory soil desiccation cracking using DLSM with a two-phase bond model

Y. Gui [a], G.-F. Zhao [b,*]

[a] Nanyang Centre for Underground Space, School of Civil and Environmental Engineering, Nanyang Technological University, 639798, Singapore
[b] State Key Laboratory of Hydraulic Engineering Simulation and Safety, School of Civil Engineering, Tianjin University, Tianjin 300072, China

ARTICLE INFO

Article history:
Received 5 March 2015
Received in revised form 1 July 2015
Accepted 1 July 2015
Available online 10 July 2015

Keywords:
Desiccation cracking
DLSM
Unsaturated soil
Two-phase bond
Heterogeneity
Particle size

ABSTRACT

The distinct lattice spring model (DLSM) is extended to modelling soil desiccation cracking by introducing a two-phase bond model. The bond, which comprises a spring bond and water bond, is developed to consider the interaction of the pore pressure with deformation of the soil matrix. A parameter representing soil heterogeneity is introduced to consider the uneven drying during desiccation. The capability of the model is demonstrated through a number of numerical examples, which are in good agreement with the experimental observations. Three significant factors controlling desiccation cracking, which are soil particle size, heterogeneity and boundary conditions, are identified.

© 2015 Elsevier Ltd. All rights reserved.

1. Introduction

Desiccation cracking is common in unsaturated soil with a high degree of saturation, which considerably increases the soil hydraulic conductivity and decreases the shear strength of the soil. Thus, it poses a significant threat to the hydraulics and structural integrity of earthworks [1], dykes [2], embankments [1,3] and engineered barriers [4,5], and it can increase the erosion potential of surface soils [1,6]. The phenomenon also has a significant impact on agricultural engineering related to the soil transportation of water, air and nutrients [7], and to groundwater system pollution [7,8]. When clearly elucidated, desiccation-induced cracking also finds applications in food engineering, process engineering, material engineering and chemical engineering.

Many numerical modelling techniques have been developed to simulate desiccation-induced cracking in soil, and they are primarily based on the finite element method (FEM) (e.g., Refs. [9–13]). Nevertheless, it is not easy to simulate cracking using a continuum-based FEM. The current simulation techniques using FEM generally preset a crack (as a weak face) or multiple cracks in a continuous medium (e.g., Ref. [13]) or they use the model boundary as a crack (e.g., Ref. [9]), which undermines the attempts to predict crack location, initiation and propagation. As an alternative, the discrete element method (DEM) (e.g., Refs. [3,14,15]) is a promising approach [14] because of its ability to capture the discrete nature of soil grains. However, the existing approaches used with DEM to simulate desiccation cracking either employ an incorrect desiccation process (e.g., Refs. [3,14]) or improperly treat the soil microstructures (e.g., Refs. [3,14,15]). Peron et al. [14] and Sima et al. [3], for example, adopted DEM to simulate the desiccation of soil; however, they adopted a particle radius change constitutive law that was incompatible with the volume change experienced at the pore-scale level.

The main objective of this paper is to extend distinct lattice spring model (DLSM) to the simulation of soil desiccation cracking by introducing a two-phase bond model that contains spring and water bonds. In the two-phase bond model, the water bond is used to represent the role of the suction during desiccation, whereas the spring bond represents the mechanical contact between soil particles. In addition, in the model, soil heterogeneity is accounted by assigning a multiplier of the water bond breakage suction value to the water bonds according to a random distribution (i.e., Weibull distribution). Various scenarios of laboratory desiccation tests, including unconstrained desiccation, linearly constrained desiccation and crack pattern tests, from the literature are simulated, and the simulation results are in good agreement with the experimental observation in all cases considered. The paper is organised as follows: in Section 2, DLSM is introduced, and the specially developed two-phase bond model is comprehensively

* Corresponding author.
E-mail address: gzhaomech@outlook.com (G.-F. Zhao).

http://dx.doi.org/10.1016/j.compgeo.2015.07.001
0266-352X/© 2015 Elsevier Ltd. All rights reserved.

described. The model is then validated via numerical modelling of the desiccation cracking of various scenarios in Section 3, and the influential factors, such as particle size and random ratio values, are investigated. Finally, the paper is summarised with a brief conclusion in Section 4.

2. The model

2.1. DLSM

In DLSM, solid media are discretised into mass particles linked by spring bonds (see Fig. 1a), comprising normal and shear springs (see Fig. 1b). Whenever two particles are detected in contact, they are linked together by the spring bonds between their centre points. The motion of the system is expressed as follows [16–18]:

$$[\mathbf{K}]\mathbf{u} + [\mathbf{C}]\dot{\mathbf{u}} + [\mathbf{M}]\ddot{\mathbf{u}} = \mathbf{F}(t) \tag{1}$$

where $\mathbf{u}$ represents the particle displacement vector, $[\mathbf{K}]$ is the stiffness matrix, $[\mathbf{M}]$ is the diagonal mass matrix, $[\mathbf{C}]$ is the damping matrix, and $\mathbf{F}(t)$ is the vector of external forces on the particles. An explicit central finite difference scheme (also call the Verlet scheme or leapfrog algorithm) is used to solve the motion equation and the calculation cycle, as shown in Fig. 1c. Hence, whenever the particle displacement is set (obtained from either the initial conditions or a previous time step), new contacts and broken bonds are detected, and the list of neighbouring particles is updated accordingly. Therefore, the particle velocity is updated individually as

$$\dot{\mathbf{u}}_i^{(t+\Delta t/2)} = \dot{\mathbf{u}}_i^{(t-\Delta t/2)} + \frac{\Sigma \mathbf{F}_j^{(t)}}{m_p}\Delta t \tag{2}$$

where $\dot{\mathbf{u}}_i^{(t+\Delta t/2)}$ and $\dot{\mathbf{u}}_i^{(t-\Delta t/2)}$ are the particle velocity at $(t+\Delta t/2)$ and $(t-\Delta t/2)$, respectively. $\Sigma \mathbf{F}_j^{(t)}$ is the sum of forces applied on the ith particle, including external forces. Therefore, the new displacement of the particle is calculated as

$$\mathbf{u}^{(t+\Delta t)} = \mathbf{u}^{(t)} + \dot{\mathbf{u}}^{(t+\Delta t/2)}\Delta t \tag{3}$$

If the displacement along the normal or shear direction is larger than a given value, spring bond breakage will be detected, and a spring bond for which only a normal spring with zero strength is defined will be applied. The failure criterion used for the spring bonds is shown in Fig. 1d, demonstrating that the bond exhibits shear and tension failure but no compression failure. The normal displacement of the spring bonds is calculated as follows:

$$\mathbf{u}_{ij}^n = (\mathbf{u}_{ij}\cdot\mathbf{n})\mathbf{n} \tag{4}$$

where $\mathbf{u}_{ij}^n$, $\mathbf{u}_{ij}$ and $\mathbf{n}$ are the normal displacement, total displacement and normal vector of the spring bond connecting particles i and j (see Fig. 1b). The normal force in the spring bond can be calculated as

$$\mathbf{F}_{ij}^n = k_n\mathbf{u}_{ij}^n \tag{5}$$

where k_n is the normal stiffness of the spring bond.

One of the distinct features of DLSM is that the relative shear displacement is obtained using the local strain of a particle group instead of the difference between the total displacement and the normal displacement, that is, $\left(\mathbf{u}_{ij}^s = \mathbf{u}_{ij} - \mathbf{u}_{ij}^n\right)$, as adopted in some conventional lattice spring models (LSMs). Thus, the shear deformation is calculated as follows [17]:

$$\widehat{\mathbf{u}}_{ij}^s = [\boldsymbol{\varepsilon}]_{bond}\cdot\mathbf{n}l - (([\boldsymbol{\varepsilon}]_{bond}\cdot\mathbf{n}l)\cdot\mathbf{n})\mathbf{n} \tag{6}$$

where l is the initial bond length or the initial distance between a pair of particles. This method overcomes the restriction on Poisson's ratio while preserving the rotational invariance, which is encountered in the traditional LSMs. Accordingly, the shear force between the particles is

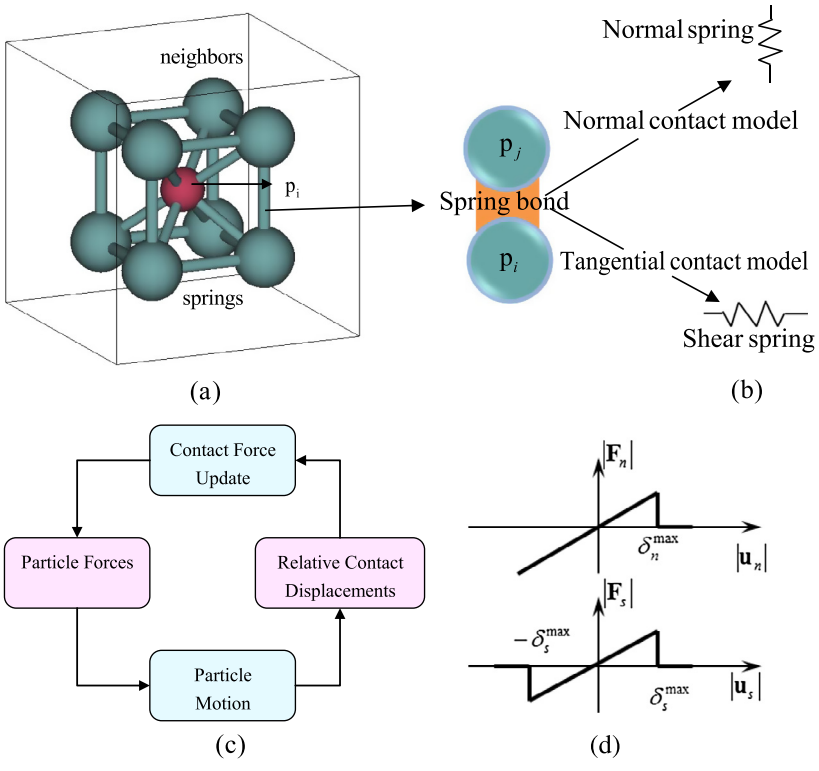

Fig. 1. (a) Physical model (b), details of the spring bond, (c) calculation flow chart of DLSM and (d) constitutive model of spring bonds (a and c are after Ref. [17] and b is after Refs. [19–22]).

$$\mathbf{F}_{ij}^{s} = k_s \hat{\mathbf{u}}_{ij}^{s} \tag{7}$$

where k_s is the shear stiffness of the spring bond. In Eq. (6), $[\boldsymbol{\varepsilon}]_{bond}$ is the bond local strain obtained by averaging the strains of the two linked particles as

$$[\boldsymbol{\varepsilon}]_{bond} = \frac{[\boldsymbol{\varepsilon}]_i + [\boldsymbol{\varepsilon}]_j}{2} \tag{8}$$

where $[\boldsymbol{\varepsilon}]_i$ is the strain matrix of the i^{th} particle and is

$$[\varepsilon] = \begin{bmatrix} \varepsilon_{xx} & \varepsilon_{xy} & \varepsilon_{xz} \\ \varepsilon_{yx} & \varepsilon_{yy} & \varepsilon_{yz} \\ \varepsilon_{zx} & \varepsilon_{zy} & \varepsilon_{zz} \end{bmatrix} \tag{9}$$

The other feature of DLSM is that the input parameters are material macro-parameters (i.e., the elastic modulus and Poisson's ratio) instead of the micro-parameters, such as the normal and shear stiffness, that are used in conventional DEMs. Because the total strain energy of the lattice model is equivalent to that of a continuum model of the same dimension, based on the Cauchy-Born rule and hyper-elastic theory, the micro-parameters adopted in DLSM can be directly calculated from the material elastic properties as follows [16,17]:

$$k_n = \frac{3E}{\alpha^{3D}(1-2\upsilon)} \tag{10}$$

$$k_s = \frac{3(1-4\upsilon)E}{\alpha^{3D}(1+\upsilon)(1-2\upsilon)} \tag{11}$$

where k_n is the normal stiffness, k_s is the shear stiffness, E is Young's modulus, υ is Poisson's ratio, and α^{3D} is the microstructure geometry coefficient, which is obtained using

$$\alpha^{3D} = \frac{\sum l_i^2}{V} \tag{12}$$

where l_i is the original length of the bond and V is the volume of the geometry model.

2.2. The two-phase bond model

According to Ref. [26], the particle forces contain three components: forces due to the applied boundary condition (transmitted through the skeleton), and particle-level forces comprising gravitational, buoyant and hydrodynamic and contact-level forces. The contact-level force includes capillary force, electrical forces and the cementation-reactive force. The first two contact-level forces can cause strains in the soil mass even at constant boundary loads. Conversely, the cementation-reactive force possibly arising from the water evaporation-induced crystal salt bond opposes skeletal deformation. Cementation is often accompanied by either shrinkage or swelling, with the ensuing changes in inter-particle skeletal forces. Under desiccation, the capillary force will vanish when the soil pore is drained. However, due to the cementation-reactive force, an attractive effect exists between particles to oppose the separation of two neighbouring particles. In the numerical model, the attractive effect can be represented by the implied attractive force of spring bond under tension. This motivates the development of the two-phase bond model.

Generally, two types of laboratory desiccation tests are used according to the external boundary conditions. These types are unconstrained and constrained desiccation tests, with the respective absence and presence of restriction on soil sample boundaries. For unconstrained desiccation shrinkage, the sample volumetric deformation can be determined by replacing the time component used in Eq. (6) in Ref. [14] with suction, which is physically more meaningful for desiccation-induced shrinkage in soil because the deformation is directly related to the suction induced by desiccation rather than time (suction and time cannot be equivalent). Therefore, the volumetric strain can be expressed as

$$\varepsilon_v = 1 - \exp(-\alpha s) \tag{13}$$

where ε_v is the shrinkage volumetric strain, $\alpha(\alpha > 0)$ is a material parameter, and s is the suction. Assuming a homogeneous deformation applied to DLSM in terms of a three-dimensional model, the force induced in the spring bond will be

$$F^s = -\frac{\varepsilon_v}{3} l k_n \tag{14}$$

where l is the original length of the spring bond and F^s is the force in the spring bond induced by deformation. To produce the given deformation, according to Newton's third law, a water bond force (F^w) representing the capillary force with the same magnitude as the force in the spring bond must be introduced. However, the water bond force is applied along the opposite orientation to the spring bond force. The water bond force is proportional to the value of suction; thus, it is calculated as

$$F^w = \beta s \tag{15}$$

Substituting Eqs. (13)–(15), the equation $\beta = \frac{(1-\exp(-\alpha s))lk_n}{3s}$ is obtained.

Fig. 2a shows the two-phase bond model. The evolution of the water bond force with suction is presented in Fig. 2b. The horizontal axis is the suction/pore pressure, and the vertical axis is the water bond force. The soil macroscopic air entry value is the suction value at which a large number of pores start to drain. Due to the heterogeneity of soil, some of the pores must be drained before the macroscopic air entry value while some can be drained after

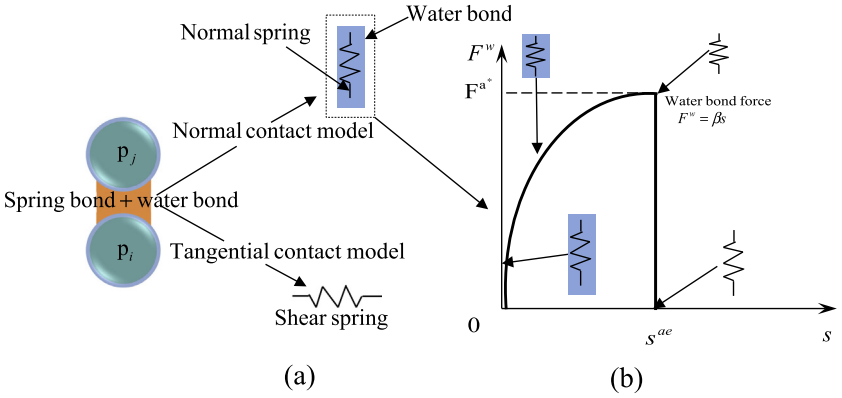

Fig. 2. Illustration of (a) model of the spring and the water bonds and (b) their constitutive model.

the macroscopic air entry value. The suction value determines the drainage of pore (i.e., water bond), which is called local water bond breakage suction. In this model, when suction reaches the water bond breakage suction value, the water bond force is reduced to zero. Taking the water bond breakage suction value into account, the criterion for water bond breakage is given as

$$F^w \geqslant F^{a^*} \tag{16}$$

where F^{a^*} is the water bond force corresponding to the water bond breakage suction value (s_{ae}); it can be calculated as $F^{a^*} = \frac{(1-\exp(-\alpha s^{se}))lk_n}{3}$.

Numerous studies have demonstrated that heterogeneity in soil in the form of soil structure, particle size, and geometry plays a significant role in soil macroscopic behaviour. These forms of heterogeneity produce an uneven evaporation surface when the soil is being desiccated, because desiccation is a continuous pore drainage process that constitutes the intrinsic cause of desiccation cracking in soil. To account for the influence of the heterogeneity, different failure parameters (e.g., the local water bond breakage suction value) are assigned to different water bonds in different spatial positions locally without using the spatial structure autocorrelation. The spatial structure autocorrelation variation has been widely used in large-scale analysis, for example slope stability [27]. The autocorrelation has not been found in use for small-scale analysis in soil, such as the laboratory desiccation test of soil. In addition, the desiccation phenomenon is dependent on the pore distribution of a soil sample, which is highly dependent on the soil grain distribution, which may be locally determined. Therefore, it is reasonable to treat laboratory desiccation phenomenon purely locally. Assuming a soil macroscopic air entry value (s_{ae}^M), which is normally obtained using laboratory tests (e.g., axial plate method), the local water bond breakage suction can be obtained using a multiplier as follows:

$$s_{ae} = \theta s_{ae}^M \tag{17}$$

where s_{ae} is the local water bond breakage suction, and θ is the multiplier of the local water bond breakage suction. The multiplier is chosen as follows:

$$\theta = \begin{cases} \gamma & \text{for breakage of local water bond} \\ \eta\gamma & \text{for the drainage of residual pore water} \end{cases} \tag{18}$$

where the parameter γ, which ranges from 0 to 1, is a random ratio obtained through a Weibull distribution [23]. η is a coefficient needed for the drainage of the residual water content in soil under desiccation. It is known that water in a pore during desiccation consists of two main parts: one is primary water and the other one is residual water. The primary water is drained once the local water bond breakage suction is reached, while the residual water describes the condition where the pore water resides primarily as isolated pendular menisci and extremely large changes in suction are required to remove additional water from the soil system. The parameter η is used to account for the drainage of the residual water. It is determined empirically. From several experiments [25], it can be seen that the residual water content is about the one-tenth of the initial water content during desiccation. Therefore, it is reasonable to assume that the residual water in each water bond could be drained when the suction value is ten times the local water bond breakage suction, because once the primary water is drained, the water bond is broken. From this point of view, the local water bond breakage suction can be replaced by:

$$s_{ae} = \gamma s_{ae}^M \tag{19}$$

In the DLSM-two-phase bond coupled model, the spring bond deformation is treated homogeneously. For a given soil, it is initially saturated, and both water and spring bonds exist between neighbouring particles (Fig. 3a). Considering desiccation under constrained boundary conditions (e.g., specified displacement), the force in the water bond gradually builds with suction as the force in the spring bond and soil volume decrease (Fig. 3b) with the progress of desiccation. No cracking will appear if all of the water bonds are broken simultaneously (Fig. 3c). However, if the water bonds fail heterogeneously, tensile deformation can form in the spring bond where the water bond has failed under the dragging force from neighbouring water bonds that have not failed yet. This may result in mechanical failure of the spring bond in the form of a crack if the tensile deformation exceeds the limit (Fig. 3d). Nevertheless, in perfectly unconstrained shrinkage, regardless of

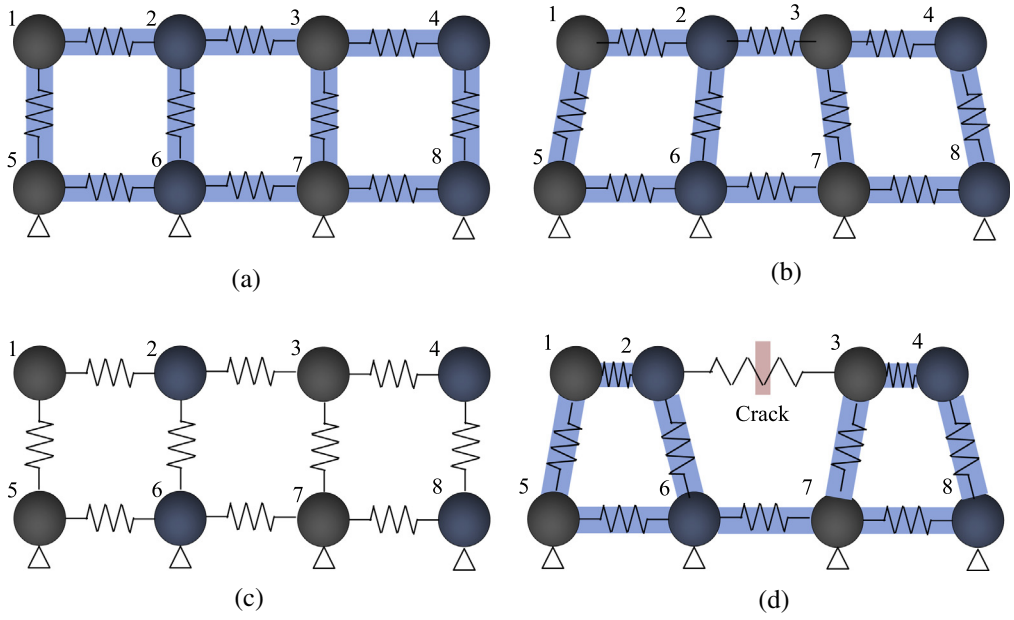

Fig. 3. Illustration of a soil crack initiation in constrained desiccation: (a) initial saturated state, (b) shrinkage deformation with desiccation, (c) homogeneous water bond failure and (d) heterogeneous water bond failure.

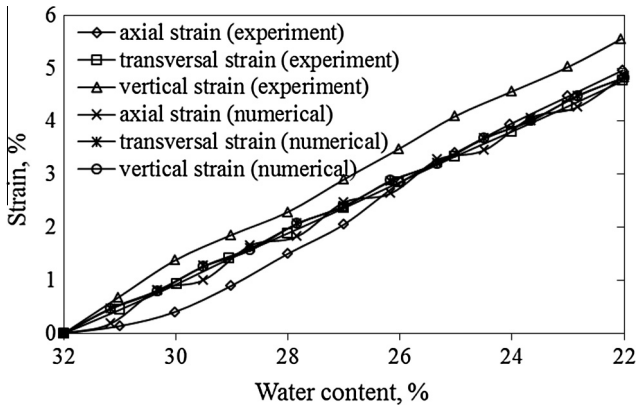

Fig. 4. Evolution of the strains with respect to the water content for the unconstrained desiccation test.

how high the negative pore water pressure (suction) is, no cracks will form because the displacement of particles is allowed and the free movement can accommodate the relaxation of the mechanical deformation of spring bonds. Therefore, the boundary condition is an external cause of desiccation cracking in soil. In general, three important factors control the cracking of soil during desiccation: the air entry value, the heterogeneity of the soil and constraints (e.g., traction or friction boundary conditions and residual stresses in the soil).

3. Numerical validations

In this section, the model is applied to simulate desiccation tests in Bioley silt [1]. The tests contained three components: unconstrained desiccation, linearly constrained desiccation and crack pattern tests. For the unconstrained desiccation test, soil slurry was poured into a mould with dimensions of $295 \times 49 \times 12$ mm and then placed on a Teflon plate to minimise friction. The environment of the test was temperature and humidity controlled, with an average relative humidity of 40% and a temperature of 19 °C with a variation of 1 °C. During desiccation, the evolution of strain with water content was measured. For the linearly constrained desiccation test, the sample size was the same as that of the unconstrained desiccation test. However, the desiccation was conducted on a notched base to create a longitudinal restraint. The testing environment of the crack pattern test was the same as in the two other tests, but the dimensions were $300 \times 300 \times 12$ mm.

3.1. Unconstrained desiccation test

The unconstrained desiccation test was used to calibrate the numerical scheme and to obtain elastic parameters. The model size was the same as the laboratory testing soil sample, that is, $295 \times 49 \times 12$ mm with an identical particle size of 2 mm. It is a cubic lattice model. The boundary condition used was that all model boundaries were kept free of any constraints. The water content ranged from 32% to 22%, which corresponded to a suction level ranging from 0 to 80 kPa. The experimental volumetric strain ε_v at the end of the test was taken to be 0.145 as the value adopted in Ref. [14], and the corresponding water content was 22% (suction level of 80 kPa from Fig. 3.17e in Ref. [13]). For the unconstrained desiccation, the longitudinal direction was considered, and the axial strain was taken to be $\varepsilon_v/3$ based on the assumption that the shrinkage is isotropic so that α could be expressed using Eq. (13) as

$$\alpha = -\frac{\ln(1-\varepsilon_v/3)}{s} = 0.0006193 \tag{20}$$

This value was used in the remaining desiccation tests. The random ratio adopted for the unconstrained desiccation was 10%. However, for unconstrained desiccation, because of the unconstrained boundary, the soil is usually saturated during the shrinkage. When the soil becomes unsaturated, the soil shrinkage almost ceases during the experimental observation [13]. Therefore, the macroscopic air entry

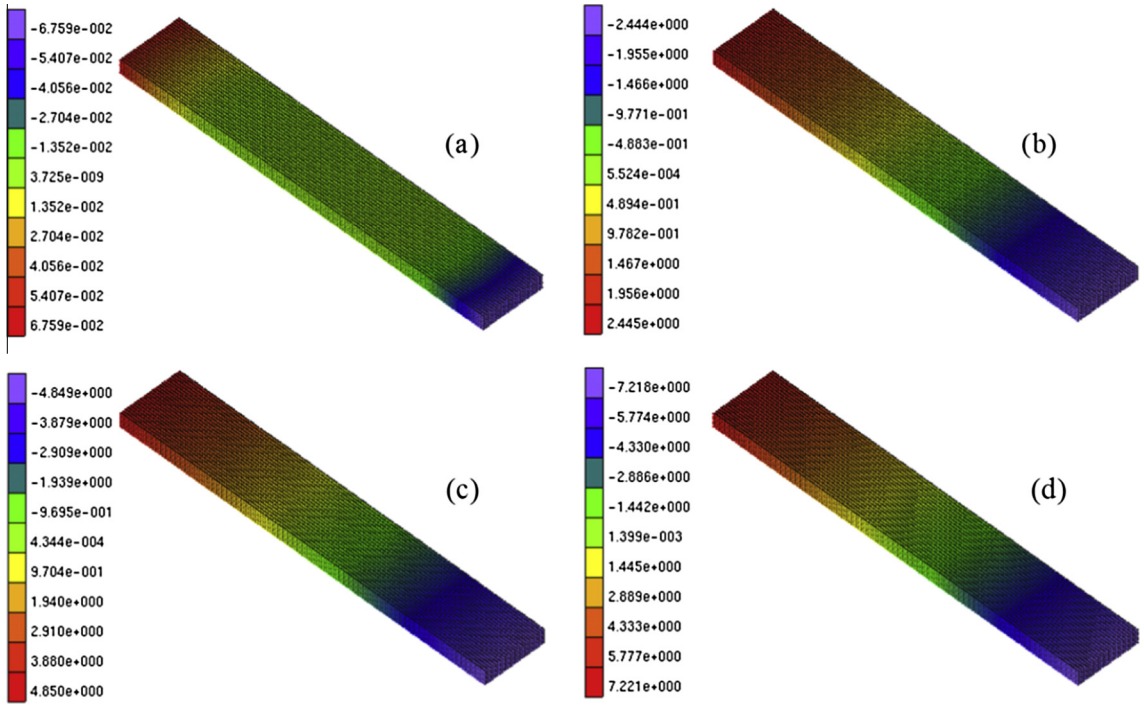

Fig. 5. Axial displacement of the unconstrained desiccation, (a) step 1 (2.7 kPa), (b) step 10 (26 kPa), (c) step 20 (52 kPa) and (d) step 30 (80 kPa).

value is not taken into account. The simulated strains with respect to the water content are shown in Fig. 4. The water content was obtained from the laboratory relationship between suction and the water content, which was almost linear in this range (see Fig. 3.17e in Ref. [13]). From Fig. 4, it can be observed that good agreement with the experimental results was attained. More specifically, all three directional strains increased nearly linearly with suction due to homogeneous shrinkage, although the soil heterogeneity had been considered in the simulation. It is worth noting that the small difference between the numerical simulation and the experimental result is from the final volumetric strain value adopted. In the simulation, a final volumetic strain of 0.145 was adopted as used in Ref. [14], while the actual final volumetric strain from the laboratory result as shown in Fig. 4 was 0.1527. In addition, because isotropic shrinkage was assumed in numerical simulation, the numerically obtained three directional strains almost overlap. Fig. 5 presents the evolution of axial displacement with suction, which increased with suction and led to larger displacement at the two extremities. The distribution of the axial displacement is almost symmetric. Although the axial displacement increased with suction, no cracking occurred. This corroborated the results of the experiments during which no cracking was observed [13] and other numerical modelling experiments [14]. Based on the modelling of the unconstrained desiccation, the elastic modulus and Poisson's ratio were calibrated to be 20 MPa and 0.2, respectively, which are close to the values obtained in laboratory from the normally consolidated test [13]. These elastic parameters are used for the rest of the simulation. Although the elastic parameters are not constants during desiccation, they are treated as constants for the current research.

3.2. Linearly constrained desiccation

The model size was the same as that of the laboratory testing soil sample, that is, 295 × 49 × 12 mm with an identical particle size of 2 mm. A random ratio of 10% is used. The boundary condition used was that displacements were prevented for the bottom particles with no restrictions for the other particles. The water bond breakage suction value of the large pores in the simulated soil was selected to be 60 kPa. In the simulation, only tensile failure was considered because desiccation cracking is primarily tensile cracking. According to the theory of DLSM (see Section 2.1), *if the*

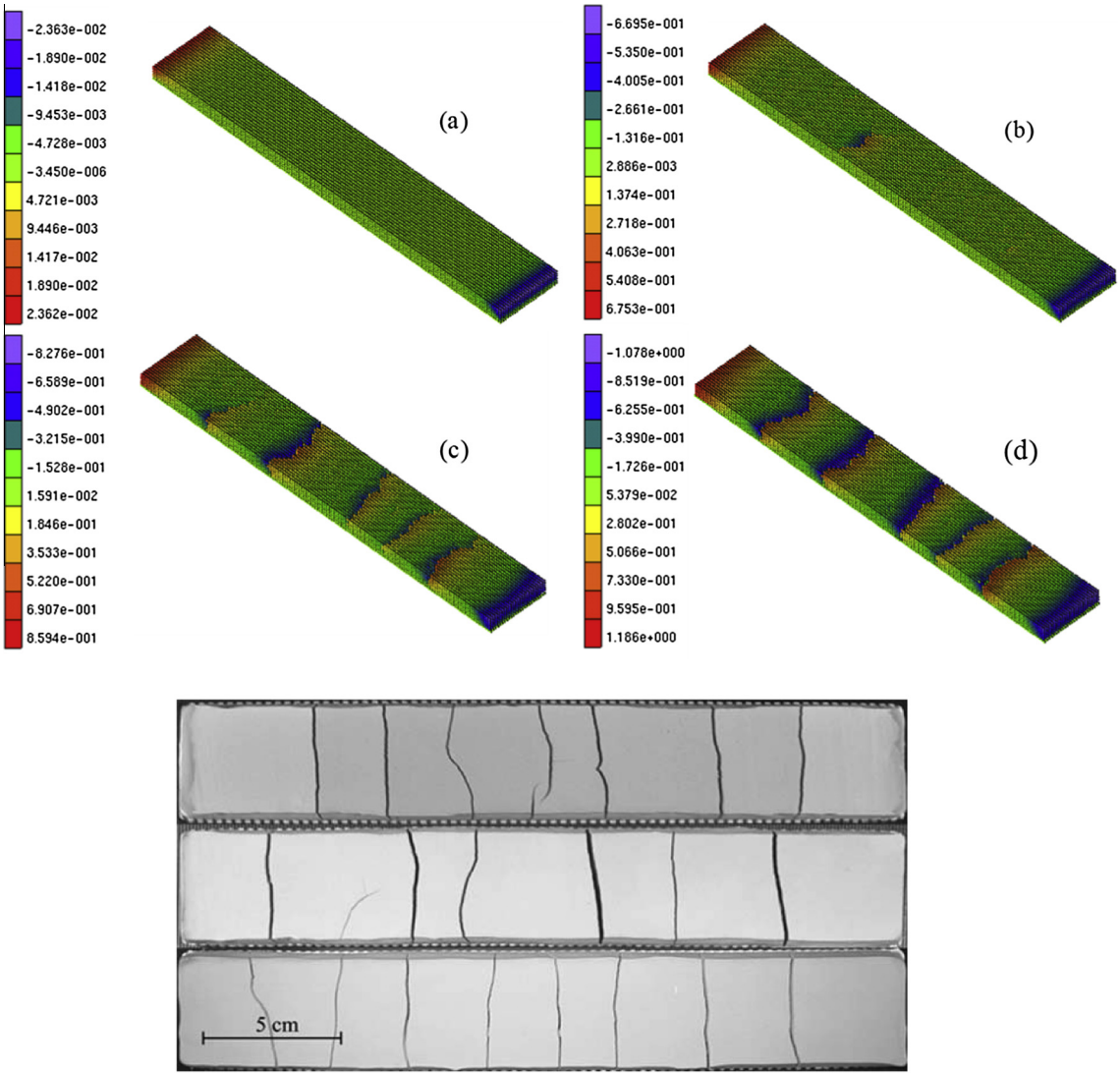

Fig. 6. Axial displacement evolution of the linearly constrained desiccation under a random ratio of 10%, (a) step 1 (2.7 kPa), (b) step 23 (61 kPa), (c) step 25 (67 kPa) and (d) step 30 (80 kPa), and (e) experimental result.

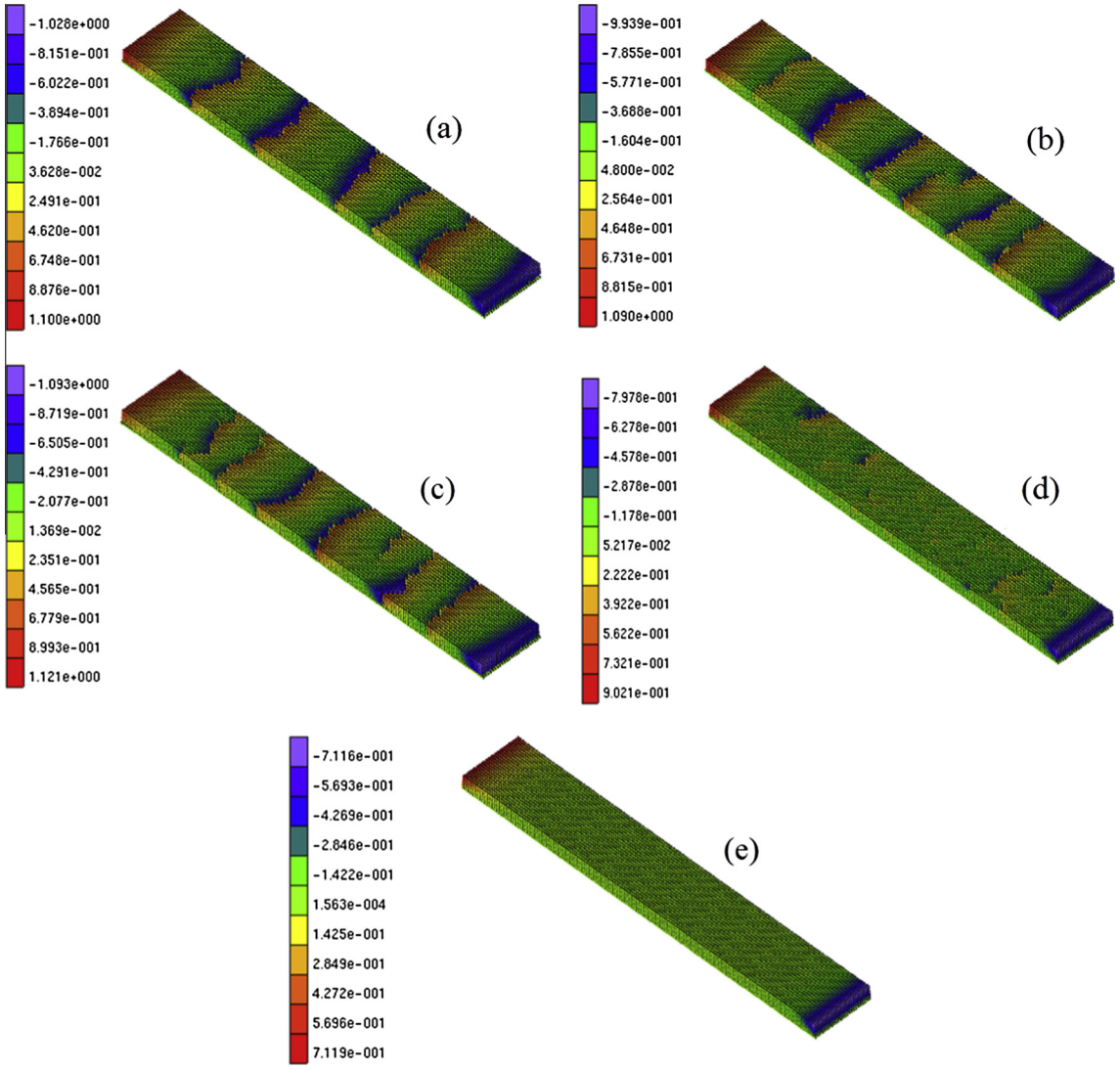

Fig. 7. Axial displacement of the linearly constrained desiccation for different degrees of heterogeneity/random ratios of (a) 5%, (b) 10%, (c) 30%, (d) 50% and (e) random ratio is zero.

displacement along the normal or shear direction is larger than a given value, the spring bond breakage will be detected, and a spring bond for which only a normal spring with zero strength is defined will be applied. Therefore, the ultimate tensile deformation of the normal spring (u_n^*) was the only failure parameter that needed to be calibrated for the constrained desiccation modelling. This parameter was obtained from a trial-and-error process. By running a number of simulations with different u_n^*, the corresponding value with the closest failure pattern to the experimental observation (i.e., the number of cracks) was selected as the calibrated value (i.e., $u_n^* = 0.00185$ mm for the 2 mm particle model). The value of u_n^* was used for the remaining constrained desiccation simulations. The random ratio selected here was 10%. Fig. 6 presents the results of the axial displacement in the modelling. The axial displacement also increased with suction. However, a number of obvious cracks occurred due to the constrained boundary condition. The cracks started from the top surface and propagated almost vertically and horizontally. In the horizontal direction, some cracks were initiated at one side boundary and propagated to the opposite side boundary (Fig. 6c). In addition, some cracks started at the middle of the top surface and then propagated to both side boundaries (Fig. 6b). In the vertical direction, the cracks propagated towards

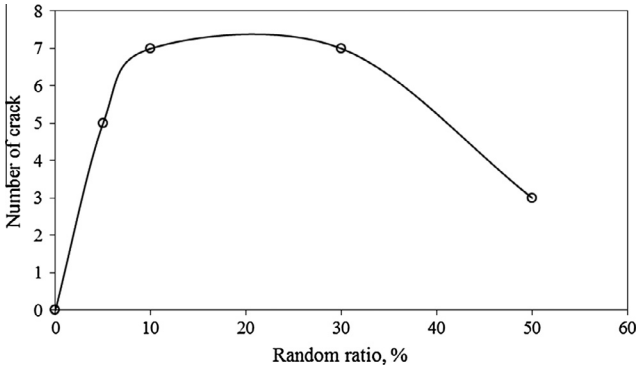

Fig. 8. The statistical crack number with random ratio (particle size is 2 mm).

the bottom, but they did not fully penetrate due to the constraints applied at the bottom boundary. As expected, with desiccation, the crack openings widened. The first crack was not initiated in the middle of the soil bar, as shown in Fig. 6(b), which differs from the prediction in Ref. [24], where the first crack was expected to

initiate in the middle of a soil bar because it was argued that the tensile stress in the middle was the highest. The current simulation results are similar to the experimental observation, as shown in Fig. 6(e).

In the uniform particle size model, one of the critical factors affecting crack patterns is the random ratio of soil, which is related to the heterogeneity of the pore size distribution (i.e., water bond in the model). In this paragraph, the effect of the random ratio on the desiccation cracking pattern is investigated. The random ratio of 50% is the most heterogeneous case, whereas the random ratio of 0% corresponds to a homogenous case in this paper. Currently, the DLSM can only qualitatively determine the random ratio that is accomplished by testing different values. Fig. 7 shows the final axial displacement for the linearly constrained desiccation simulations using five different random ratios, that is, 5%, 10%, 30%, 50% and 0%, respectively for (a), (b), (c), (d), and (e). The desiccation crack patterns are closely related to the random ratio of the water bond. Generally, a higher random ratio indicates that the observed cracks are more frequent and smaller. When the random ratio reaches 50%, all of the cracks become smaller and more complicated. However, if all of the water bonds are distributed homogeneously, then a random ratio of 0% is obtained. In this case, no desiccation cracks are created (see Fig. 7e). More specifically, the relationship between the random ratio and number of cracks in this study is quantitatively presented in Fig. 8. The crack number initially increases from zero to seven with five and seven cracks, respectively for random ratio of 5–10%. However, if the random ratio continues to increase to 50% which represents the most heterogeneous scenario, the number of cracks decreases again to three. It is worth noting that the crack is counted once it is observable.

Particle size is another factor that significantly affects the desiccation crack pattern in soil. The determination of the proper particle size in the model is also qualitative, and it should be calibrated

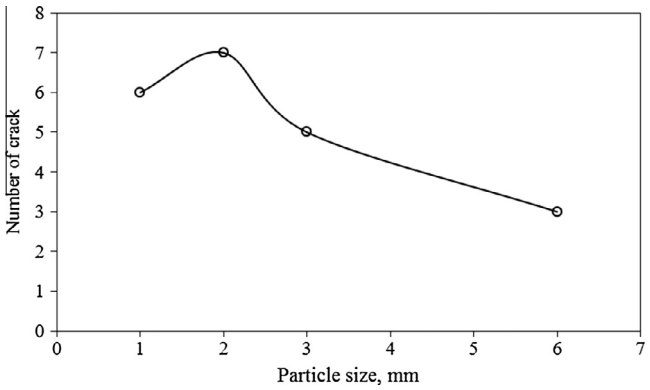

Fig. 10. Statistical crack number with particle size (random ratio is 10%).

with the random ratio for the cracking observed in a controlled test case. The choice of the particle size is typically controlled by the capacity of the computational environment. For a given volume of soil, more particles must be created if a higher resolution of the numerical results is desired. Fig. 9 shows the influence of the particle size on the crack pattern. For a given random ratio (i.e., 10%), models with smaller particles lead to greater formation of soil cracks. Fig. 10 presents the quantitative relationship of the crack number and particle sizes investigated in this paper. Three imperceptible cracks are formed when the particle size is 6 mm; however, this number increases and reaches to seven when the particle size decreases to 2 mm. For the particle size of 1 mm, the obtained crack number is six. For any problem of interest. this finding implies that the desired number of regular particles can be satisfactorily obtained by adjusting the value of the random ratio to match the crack pattern observed in the calibration test case of the problem.

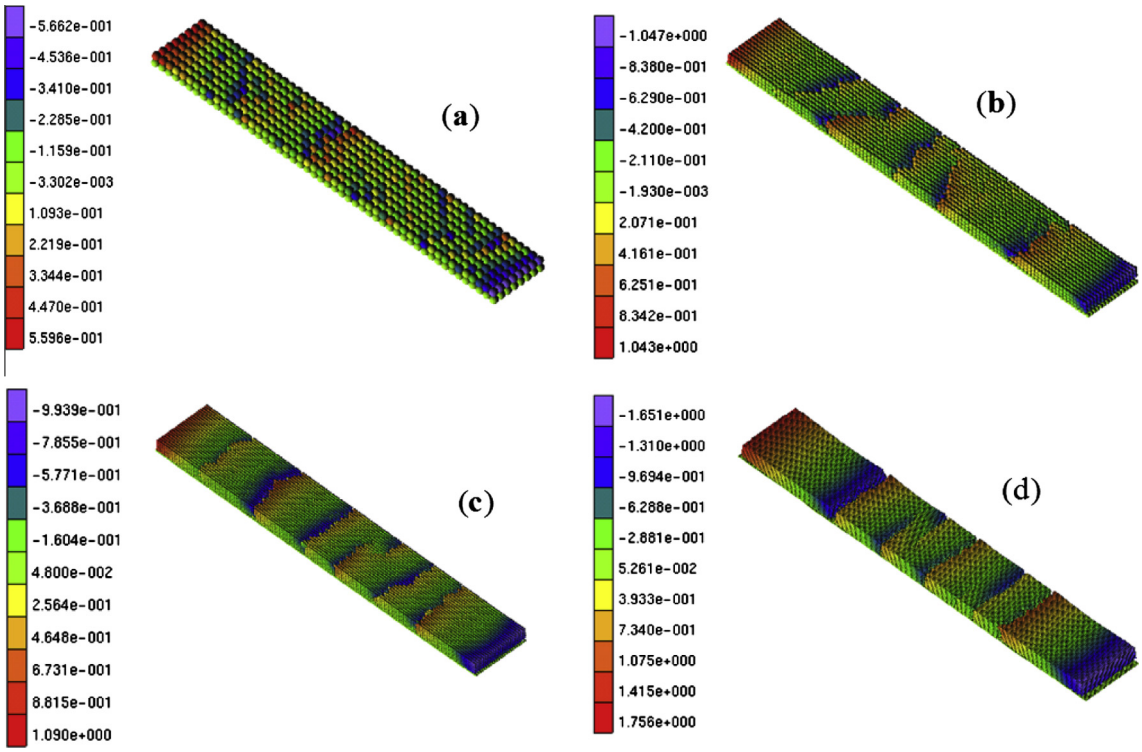

Fig. 9. Axial displacement of the linearly constrained desiccation with particle size of (a) 6, (b) 3, (c) 2 and (d) 1 mm under a random ratio of 10%.

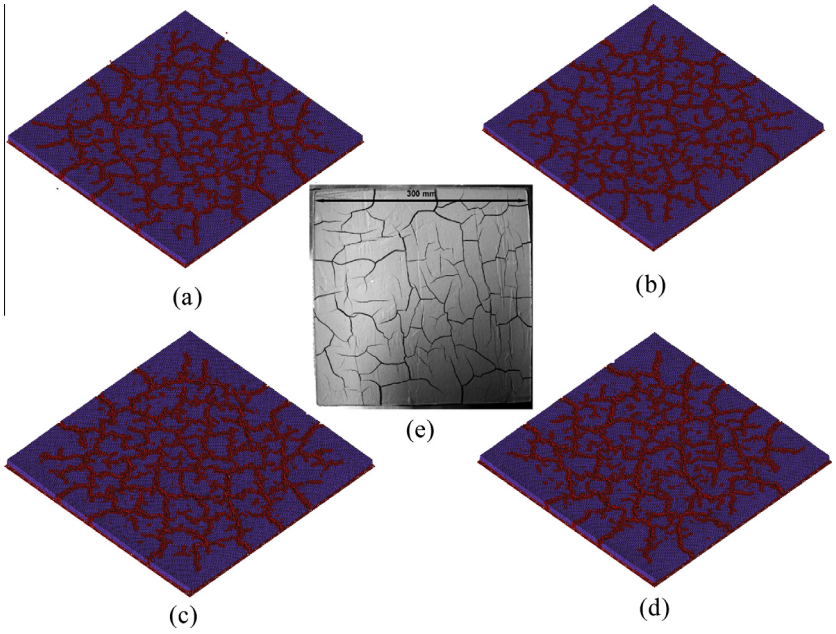

Fig. 11. Comparison of (a–d) the 3D crack pattern simulation results (random ratio is 10%) with (e) the experimental result.

3.3. Crack pattern simulation

Based on the unconstrained and linear constrained desiccation simulations, the elastic parameters (i.e., elastic modulus and Poisson's ratio) and failure parameter (i.e., critical normal displacement of the spring bond) of the model for Bioley silt were established. These parameters were also applied in the crack pattern simulation.

For the simulation, a square slab model was built. The model had the same dimension as the experimental sample, which was $300 \times 300 \times 12$ mm, with identical particles of 2 mm. Therefore, the model comprised 135,000 particles. A random ratio of 10% was used for the simulation. Fig. 11 presents a comparison of the simulation and the experimental result. The network in red colour in Fig. 11a represents the crack network, which is in good agreement with the experimental result (see Fig. 11b). The cracks always intersect each other at approximately right angles or 120°. Right angles are formed because the tensile stress along the direction perpendicular to the current crack paths is the largest. The intersections at 120° occur to create the minimum crack surface and energy loss in a unit volume of soil. These are consistent with the observation results in Refs. [10,13].

4. Conclusions

In this paper, a two-phase bond model is introduced into the DLSM to simulate desiccation shrinkage and cracking in soil. The model considers the interaction of the pore pressure with the deformation of the soil matrix by applying a water bond theory. Compared with the existing particle size shrinking model (e.g., Refs. [3,14]), the proposed two-phase bond model is a more physically appropriate treatment for desiccation shrinkage and cracking. In the particle size shrinking model, the particle size decreases as a function of time. However, in real soil desiccation, the soil volume shrinks because the soil matrix is deformed, rather than the soil particles. The proposed coupled DLSM with two-phase bond model is verified against the experimental results. The numerical simulation and the experimental data are in good agreement for the different scenarios considered. From the modelling, three essential factors that control desiccation cracking in soil are verified, that is, air entering the soil, heterogeneity and boundary conditions of the soil sample during desiccation.

Acknowledgements

The authors would like to thank the anonymous reviewers for very carefully reading and providing valuable comments on the paper, which have greatly improved the paper.

References

[1] Peron H, Hueckel T, Laloui L, Hu LB. Fundamentals of desiccation cracking of fine-grained soils: experimental characterisation and mechanisms identification. Can Geotech J 2009;46(10):1177–201.
[2] Philip LK, Shimell H, Hewitt PJ, Ellard HT. A field-based tests cell examining clay desiccation in landfill liners. Q J Eng Geol Hydrogeol 2014;35:345–54.
[3] Sima J, Jiang M, Zhou C. Numerical simulation of desiccation cracking in a thin clay layer using 3D discrete element modelling. Comput Geotech 2014;56:168–80.
[4] Rayhani MHT, Yanful EK, Fakher A. Desiccation-induced cracking and its effect on the hydraulic conductivity of clayey soils from Iran. Can Geotech J 2007;44:276–83.
[5] Dixon D, Chandler J, Graham J, Gray MN. Two large-scale sealing tests conducted at Atomic Energy of Canada's underground research laboratory: the buffer-container experiment and the isothermal test. Can Geotech J 2002;39(3):503–18.
[6] Intharasombat N, Puppala AJ, Williammee R. Compost amended soil treatment for mitigating highway shoulder desiccation cracks. J Intrastruct Syst 2007;13(4):287–98.
[7] Arnold JG, Potter KN, King KW, Allen PM. Estimation of soil cracking and the effect on surface runoff in a Texas Blackland Prairie watershed. Hydrol Process 2005;19:589–603.
[8] Kissel DE, Ritchie JT, Burnett E. Nitrate and chloride leaching in a swelling soil. J Environ Qual 1974;3(4):401–4.
[9] Shen Z, Deng G. Numerical simulation of crack evolution in clay during drying and wetting cycle. Rock Soil Mech 2004;25:1–7.
[10] Youshida S, Adachi K. Numerical analysis of crack generation in saturated deformable soil under row-planted vegetation. Geoderma 2004;120:63–74.
[11] Peron H, Hu LB, Laloui L, Hueckel T. Numerical and experimental investigation of desiccation of soil. In: 3rd Asian Conference on Unsaturated Soils, Nanjing, China; 2007.
[12] Trabelsi H, Jamei M, Zenzri H, Olivella S. Crack patterns in clayey soils: experiments and modelling. Int J Numer Anal Meth Geomech 2012;36:1410–33.
[13] Peron H. Desiccation cracking of soils. PhD thesis. École Polytechnique Fédérale de Lausanne, Switzerland; 2008.

[14] Peron H, Delenne JY, Laloui L, El Youssoufi MS. Discrete element modelling of drying shrinkage and cracking of soils. Comput Geotech 2009;36:61–9.
[15] Kharaghani A, Metzger T, Tsotsas E. An irregular pore network for convective drying and resulting damage of particle aggregates. Chem Eng Sci 2012;75:267–78.
[16] Zhao GF. Development of micro-macro continuum-discontinuum coupled numerical method. PhD thesis. École Polytechnique Fédérale de Lausanne, Switzerland; 2010.
[17] Zhao G, Fang J, Zhao J. A 3D distinct lattice spring model for elasticity and dynamic failure. Int J Numer Anal Met 2011;35:859–85.
[18] Zhao GF, Russell AR, Zhao X, Khalili N. Strain rate dependency of uniaxial tensile strength in Gosford sandstone by the Distinct Lattice Spring Model with X-ray micro CT. Int J Solids Struct 2014;51:1587–600.
[19] Jiang MJ, Leroueil S, Konrad JM. Insight into strength functions of unsaturated granulates by DEM analysis. Comput Geotech 2004;31(6):473–89.
[20] Jiang MJ, Leroueil S, Konrad JM. Yielding of microstructured geomaterial by Distinct Element Method analysis. J Eng Mech (ASCE) 2005;131(11): 1209–13.
[21] Jiang MJ, Yu H-S, Leroueil S. A simple and efficient approach to capturing bonding effect in naturally microstructured sands by Discrete Element Method. Int J Numer Meth Eng 2007;69:1158–93.
[22] Jiang MJ, Yu H-S, Harris D. Bond rolling resistance and its effect on yielding of bonded granulates by DEM analyses. Int J Numer Anal Meth Geomech 2006;30(7):723–61.
[23] Weibull W. A statistical distribution function of wide applicability. J Appl Mech 1951;18:293–7.
[24] Kodikara JK, Choi X. A simplified analytical model for desiccation cracking of clay layers in laboratory tests. In: 4th International conference on unsaturated soils. American Society of Civil Engineers, Carefree, AZ, United States; 2006. p. 2558–69.
[25] Lu N, Likos WJ. Unsaturated soil mechanics. Hoboken (New Jersey): John Wiley & Sons Inc.; 2004.
[26] Santamarina J. Soil behavior at the microscale: particle forces. Soil Behav Soft Ground Constr 2003:25–56. http://dx.doi.org/10.1061/40659(2003) 2.
[27] Ji J, Liao HJ, Low BK. Modeling 2-D spatial variation in slope reliability analysis using interpolated autocorrelations. Comput Geotech 2012;40:135–46.